Type of contribution:
Editorial
▶ Research Paper
Case Study
Review Paper
Scientific Data
Report of Tech. Application

e-issn. 2798-5245

Mechanical Engineering for Society and Industry
Vol. 6, No. 1 (2026) pp 128-145
https://doi.org/10.31603/mesi.15393

Improving the thermal efficiency of fin-tube heat exchangers by optimizing geometric parameters of curved rectangular winglet vortex generators

Dan Mugisidi[1]*, Oktarina Heriyani[1], Amir Khalid[2], Ahmed Rahmani[3]

[1] Department of Mechanical Engineering, Faculty of Industrial and Informatics Technology, Universitas Muhammadiyah Prof DR HAMKA, Jakarta Timur 13830, **Indonesia**
[2] Faculty of Mechanical and Manufacturing Engineering, Universiti Tun Hussein Onn Malaysia, Batu Pahat, Johor, Malaysia
[3] Sustainable Development and Environmental Protection Laboratory, Larbi Ben M'hidi University, Oum El Bouaghi, 04000, **Algeria**
✉ dan.mugisidi@uhamka.ac.id

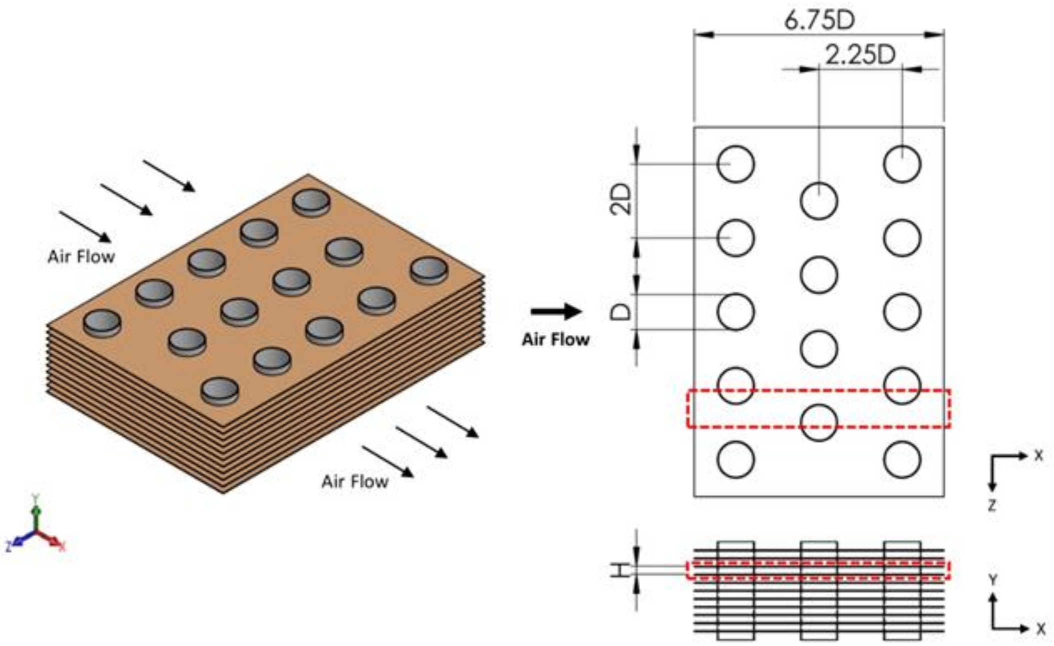

Highlights:

- Curved rectangular winglet vortex generators (CRW-VGs) were optimized to improve the thermal enhancement factor in fin–tube heat exchangers.
- Computational fluid dynamics analysis showed that radial distance, hole width, and angular position strongly influence heat transfer and pressure drop behavior.
- Smaller radial distances enhanced TEF by suppressing mixing vortices, while larger hole widths improved heat transfer through stronger jet-flow generation.
- The optimum configuration achieved a maximum TEF of 1.075 at an angular position of 120°, hole width of 0.5 H, and radial distance of 1.25.
- The findings demonstrate that proper geometric optimization of vortex generators can enhance heat transfer performance while minimizing pressure drop penalties.

Article info
Submitted: 2025-11-20
Revised: 2026-03-23
Accepted: 2026-04-06

Publisher
Universitas Muhammadiyah Magelang

Abstract
Thermal efficiency is a fundamental criterion in the design and operation of heat exchangers because it provides a clear view of the thermal behaviour and reliability of the system. Integrating vortex generators (VGs) with heat exchangers often increases turbulence and enhances the heat transfer rate but at the cost of increased pressure drops. This study aims to maximise the thermal enhancement factor (TEF) in fin–tube heat exchangers by optimising the radial distance, hole width and angular position of curved rectangular winglet vortex generators (CRW-VGs). Computational

fluid dynamics analysis is utilised to investigate how variations in radial distance and hole width influence CRW-VG performance. Parameters such as TEF, Nusselt number ratio, friction factor ratio and flow regime were examined. The results show that smaller radial distances suppress mixing vortices and enhance TEF, while larger hole widths generate strong jet flows and increase heat transfer rates. The highest TEF of 1.075 is achieved at an angular position of 120°, a hole width of 0.5 H and a radial distance of 1.25. The study reveals that optimising the geometric parameters of VGs is proven satisfactory for enhancing heat transfer performance and minimising pressure drop.

Keywords: Curved rectangular winglet; Heat transfer enhancement; Hole width; Radial distance; Vortex generator

1. Introduction

Thermal efficiency is a crucial aspect in the design and operation of heat exchanger systems, playing an essential role in various industrial applications, such as power generation, cooling and chemical processing [1]. The need for better heat exchange in these systems with more compact designs has resulted in much research on this topic.

Air is the common working fluid in fin–tube heat exchangers. Similar to all gases, air has relatively poor thermophysical properties for heat transfer [2]. This limitation prompted researchers to enhance the effectiveness of heat transfer systems to increase energy efficiency while lowering production costs. Enhancing the air-side heat transfer of these equipment has been the subject of several theoretical, numerical and experimental investigations. A proven effective solution is the integration of vortex generators (VGs). These small devices are designed to enhance aerodynamic performance, flow control and heat transfer in forced draft cooling towers [3]. VGs improve thermal performance by inducing subsidiary currents, disrupting interface region development and promoting fluid dispersion near the walls. The longitudinal vortices generated by VGs allow reduced stagnation zones behind the tubes [4], increase turbulence intensity and well fluid mixing [5]. Increasing turbulence often enhances the heat transfer rate but at the cost of increased pressure drops. Therefore, optimising heat transfer and reducing fluid flow resistance have become the primary focus.

Previous studies have demonstrated that both the placement and geometric configuration of VGs significantly influence the thermal–hydraulic performance of fin–tube heat exchangers. Positioning VGs near the centre of the tube has been shown to provide more effective heat transfer enhancement compared with inlet or outlet placements, primarily due to the stronger interaction between the generated vortices and the tube wake region [6], [7]. In addition, smaller VG geometries operating at lower Reynolds numbers have been reported to further improve heat exchange performance [8].

Geometric optimisation of the heat exchanger structure also plays an important role in determining overall performance. The optimal combination of a larger fin pitch and a smaller tube diameter has been experimentally identified as providing improved fluid flow characteristics [9]. However, increasing the fin pitch can reduce the Nusselt number (Nu) and the wall friction factor (f) because of weakened vorticity formation and enhanced turbulent energy dissipation [10]. Furthermore, numerical investigations have shown that combining concave and convex VG surfaces generates stronger longitudinal vortices, resulting in an enhancement of the heat transfer rate of approximately 14.4% [11].

Operational parameters, such as VG location and angle of attack (AoA), further determine heat transfer effectiveness. Higher attack angles, particularly when VGs are positioned farther from the tube, can substantially increase heat transfer rates [12]. Conversely, smaller angles may be advantageous in certain configurations by directing colder fluid towards weak wake regions [13]. An AoA of 45° has consistently been identified as providing superior thermal enhancement compared with other angles [14], [15]. Furthermore, increasing the number of staggered VGs enhances the thermal enhancement factor (TEF) by accelerating flow and promoting fluid mixing in the wake region [16], [17]. These configurations are commonly arranged in common flow up, common flow down (CFD) or hybrid arrangements to optimise performance.

In rectangular channel systems, geometric parameters, such as winglet aspect ratio and channel height (H), have been identified as the dominant factors affecting heat transfer performance [18], [19]. Increasing duct height significantly alters vortex development, especially when VGs are mounted on opposing walls, thereby enhancing overall flow dynamics and heat transfer efficiency. Heat exchange performance is also highly sensitive to VG position and geometry

[20], with even minor geometric changes producing noticeable variations in performance [21], [22].

Among the various structural innovations, perforated VGs have emerged as a promising approach for improving thermal performance [23]. Perforated rectangular winglets have been reported to increase the Nu by approximately 3.91–5.52 times, achieving a maximum thermal performance factor of 2.01 [24]. Similarly, double perforated inclined elliptic turbulators have demonstrated Nu enhancements of up to 217.4% [25]. These improvements are attributed to jet flows generated through perforations, which disrupt recirculation zones and intensify fluid mixing, thereby enhancing thermal exchange efficiency [26], [27], [28].

Despite these substantial advancements, existing studies predominantly emphasise external geometric modifications, placement strategies and angle of attack variations. Although perforating the VG surface can either enhance or deteriorate heat transfer performance, depending on the hole size, number and placement, because it changes the vortex strength and the pressure drop [29], systematic investigations of hollow rectangular winglet VGs remain limited. More importantly, the geometric perforation parameter (hole width) and the positional parameter (radial distance from the tube) have largely been examined independently. Consequently, the coupled interaction between these two design variables and their combined influence on thermal–hydraulic performance has not been comprehensively evaluated. This lack of integrated parametric analysis restricts the development of optimised hollow VG configurations capable of simultaneously maximising heat transfer enhancement and minimising pressure drop penalties. To overcome this limitation, this study proposes a performance-based geometric optimisation framework for circular ring winglet vortex generators (CRW-VGs) in fin–tube heat exchangers, focusing on radial distance and hole width as key design variables.

The coupled effects of radial distance (r/R = 1.25 and 1.5) and hole width (0.25 *H* and 0.5 *H*) are systematically analysed using high-fidelity CFD simulations. Performance is evaluated through integrated metrics, including the TEF, Nu/Nu_o, friction factor ratio (f/f_o) and flow structure characterisation. By integrating geometric sensitivity analysis with unified thermo-hydraulic evaluation and mechanistic interpretation of vortex dynamics, this study identifies the optimal configuration that maximises heat transfer while minimising pressure drop, providing both quantitative assessment and mechanistic insight for a compact heat exchanger design.

2. Methodology

2.1. Physics Model

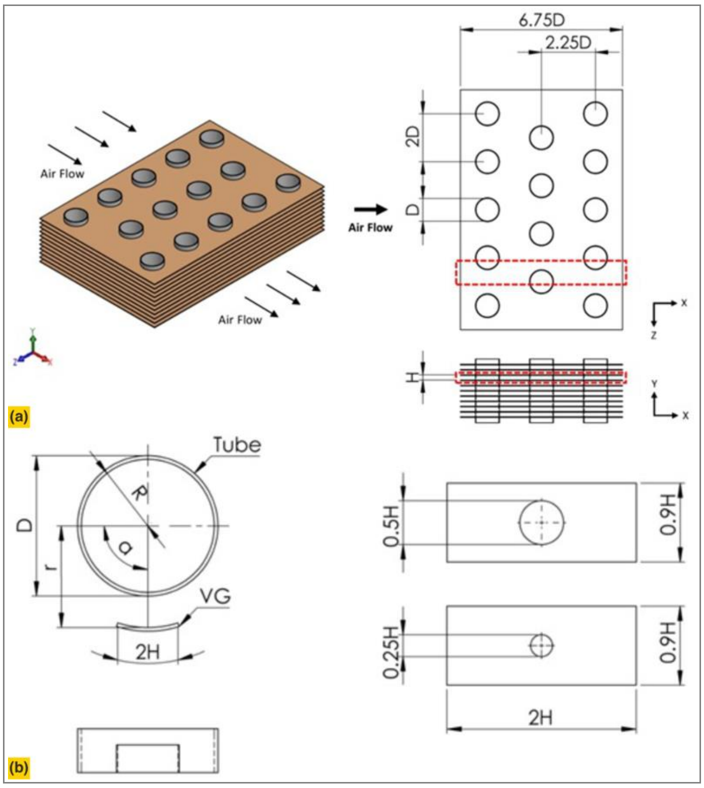

Figure 1. Schematic illustration and the main dimensions of the studied VG: (a) The overall configuration of the fin–tube heat exchanger; (b) Detailed geometry of the CRW-VG

Figure 1 shows the geometric details of a heat exchanger with three rows of staggered tubes. The VGs employed in this study take the form of a rectangular curved winglet design characterised by the geometry depicted in **Figure 1**. **Figure 1a** presents the overall configuration of the fin–tube heat exchanger and the computational domain employed in the CFD simulations. The three-dimensional (3D) schematic depicts the staggered tube arrangement and the direction of airflow. The top view specifies the tube pitches: the transverse pitch, PT = 2.25 D and the longitudinal pitch, PL = 6.75 D, where D denotes the outer tube diameter. The side view defines H as the vertical distance between two adjacent fins. The dashed rectangular region marks the representative segment selected from the complete heat exchanger geometry for numerical modelling. The tube radius, R = D/2, serves as the reference length for positioning analysis. **Figure 1b** shows the detailed geometry of the CRW-VG. The winglet length in the streamwise direction is 2 H, which is twice that of H. The winglet height is 0.9 H, providing a small clearance from the fin surface to prevent excessive blockage. Perforated configurations use circular holes with diameters of 0.5 *H* and *0.25 H*, representing the large, medium and small perforation cases, respectively, examined in the parametric study. All geometric dimensions are normalised by H for geometric similarity and scalable comparison.

This model serves as a pivotal component in our experimental setup, aimed at investigating its effects on enhancing fluid dynamics and heat transfer processes. The geometry of the VGs, as illustrated in the figure, showcases its distinctive features and potential to induce vortices and modify the flow field. Due to its efficacy in improving the performance of various thermal systems, such VG configurations have been widely studied [19], making them ideal candidates for our research endeavours. By using this specific design, this study aims to elucidate the VGs' impact on the efficiency and effectiveness of heat transfer mechanisms within our experimental apparatus.

The main dimensions refer to Oh and Kim's previous investigation [30]: diameter *D* = 32 mm, length *L* = 6.75, longitudinal pitch *P_L* = 2.25*D*, transverse pitch (*P_T*) = 2*D*, *H* = 7 mm, length of the section with radius 2 *H* and corner radius 60º. The hole widths of the CRW-VGs are 0.25 *H* and 0.5 *H*, with a VG height of 0.9 *H*. The angular position (α) indicates the angle measured in an anticlockwise manner from the lengthwise orientation of the tube to the line linking the CRW-VGs to the central point of the tube, (*r*) denotes the distance measured radially from this central point, and *R* represents the radius of the tube. The investigation of these parameters was carried out using variations in position angles (α): 30°, 45°, 60°, 75°, 90°, 105°, 120°, 135° and 150° with *r*/*R* = 1.25 and 1.5.

2.2. Governing Equation

The flow conditions in the system under investigation are assumed to be incompressible, indicating that changes in density due to pressure variations are negligible and do not significantly alter the fluid's behaviour. In the fin tube heat exchanger, a Newtonian fluid with a constant stream is employed. The conservation equations for mass, momentum and energy are expressed as follows:

$$\nabla \cdot \vec{V} = 0 \tag{1}$$

$$\rho(\vec{V} \cdot \nabla)\vec{V} = -\nabla p + \mu\nabla^2\vec{V} \tag{2}$$

$$\rho\vec{V} \cdot \nabla h = \nabla \cdot (k\nabla T) \tag{3}$$

The notation in the equation above equations, namely $\vec{V}$, ρ, p, h, k, μ, and T involved are the velocity vector, air density, static pressure, thermal conductivity of air, dynamic viscosity, and static temperature, respectively.

The heat transfer performance (TEF) is formulated as follows [31],

$$TEF = (Nu/Nu_0)/(f/f_0)^{1/3} \tag{4}$$

where the Nusselt number (*Nu*) and friction factor (*f*) are formulated as follows.

$$Nu = hL_c/k \tag{5}$$

$$f = 2\Delta pH/(\rho U_c^2\, L) \tag{6}$$

2.3. Computational Domain and Boundary Conditions

Figure 2 illustrates the computational domain of the fin–tube heat exchanger equipped with CRW-VGs. The domain represents the lateral arrangement, flow direction and fin pitch orientation. Owing to geometric uniformity and cyclic configuration, the computational region is defined as half of the transverse pitch (P_T/2) in the x-direction and one full pitch length in the z-direction. This periodic simplification significantly reduces computational costs while preserving the essential flow and heat transfer characteristics.

To ensure an accurate representation of the physical system, steady-state and incompressible flow assumptions are adopted. The domain is extended sufficiently in the streamwise direction to allow proper flow development and to avoid undesirable numerical or physical instabilities.

2.3.1. Boundary conditions

At the inlet, a uniform velocity profile and a constant temperature are specified:

$$\mathrm{u} = (u_{in}, 0, 0), T = T_{in} \tag{7}$$

where u is the velocity vector, u_{in} is the inlet air velocity, and T_{in} is the inlet air temperature.

At the outlet, a constant reference pressure is prescribed:

$$p = p_{out} \tag{8}$$

together with zero-gradient conditions for velocity and temperature:

$$\frac{\partial \mathrm{u}}{\partial n} = 0, \frac{\partial T}{\partial n} = 0 \tag{9}$$

where n denotes the outward normal direction to the outlet boundary.

For all solid surfaces, including the tube, fins, and CRW-VGs, the no-slip condition is applied:

$$\mathrm{u} = 0 \tag{10}$$

A constant wall temperature is imposed on the tube surface:

$$T = T_w \tag{11}$$

where T_w is the prescribed tube wall temperature.

Due to the periodicity of the geometry in the transverse and spanwise directions, periodic boundary conditions are employed:

$$\phi(x, y, z) = \phi(x, y, z + P) \tag{12}$$

where ϕ represents the dependent flow variables (velocity components, pressure and temperature), and P denotes the periodic pitch length.

These boundary conditions ensure physically consistent flow development and reliable prediction of heat transfer and fluid flow characteristics within the computational domain.

Matching boundary conditions are established in the x orientation amid the algorithmic region, while cyclic restrictions are established on both the higher and lower surfaces in the upriver and downriver orientations. The wing region incorporated into the CRW-VGs serves as a barrier, and the tube is subjected to constraints at this enclosure. These conditions ensure stable flow patterns within the algorithmic region, preventing undesired turbulence or instability. Moreover, the no-slip conditions and consistent surface temperature facilitate precise control and optimise the flow dynamics around the wing region and tube enclosure.

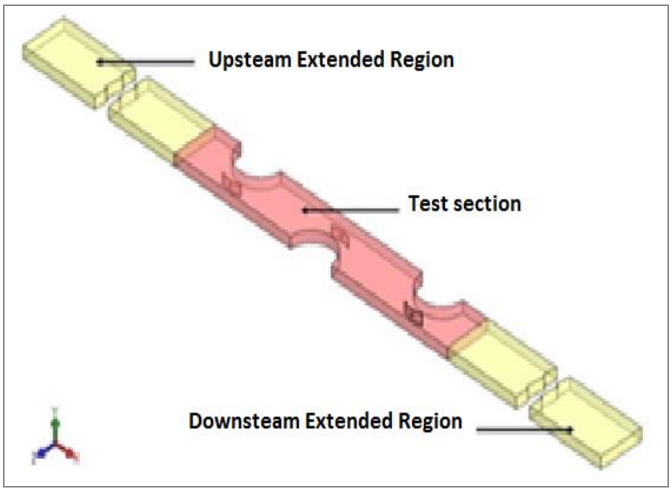

Figure 2. Computational domain

2.4. Convergence Assessment

The convergence of the numerical solution was assessed using a combination of residual-based, physical-based and grid-independence criteria to ensure numerical accuracy and physical reliability.

The normalised residuals of the governing equations were monitored during the iterative process. Convergence was assumed when the residuals of the continuity and momentum equations decreased below 10^{-6}, while a stricter threshold of 10^{-8} was imposed for the energy equation due to the heat transfer-oriented nature of the present study.

In addition to residual monitoring, several global physical quantities were continuously tracked, including the average Nusselt number ($\mathrm{Nu}_{\mathrm{\_avg}}$), f and outlet bulk temperature ($\mathrm{T}_{\mathrm{out}}$). The solution was considered physically converged only when the relative variation in these parameters over 500 successive iterations was satisfied:

$$\left| \frac{\phi^{(n)} - \phi^{(n-500)}}{\phi^{(n)}} \right| < 0.1\% \tag{13}$$

where ϕrepresents $\mathrm{Nu}_{\mathrm{\_avg}}$, f, or $\mathrm{T}_{\mathrm{out}}$, and $\mathrm{n}$denotes the iteration number.

Furthermore, a grid independence study was conducted using four progressively refined meshes ranging from 600,641 to 915,422 elements. The relative deviations of $\mathrm{Nu}_{\mathrm{\_avg}}$ and f between the two finest meshes were below 0.1%, confirming mesh independence. This value is well within the commonly accepted convergence range of 1%–2% [32]. Thus, the grid with 822,157 elements was adopted for all subsequent simulations to achieve an optimal balance between numerical accuracy and computational efficiency.

2.5. Grid Independence Test

A grid independence test was carried out for numerical analysis. The computational grid was bifurcated into two parts, specifically the region adjacent to the VGs and the rest of the area. The non-conformal interface approach was implemented between these two zones. To ensure accuracy in analysis and attain optimal grid quality, grid generation employed inflation techniques in the tube vicinity and VGs. As illustrated in **Figure 3**, the cell geometry utilised around the VGs is tetrahedral because the element can precisely capture arbitrary flow around the complex geometry of the VG [33] and is directly relevant to finely detailed VGs. Four different grid sizes are considered in **Table 1** to list the number of cells.

Table 1. Grid independence test

Number of grids	*Nu_avg*	*f*
600,641	16.55447	0.09671
715,421	16.70175	0.09603
822,157	16.79783	0.09551
915,422	16.80972	0.09549

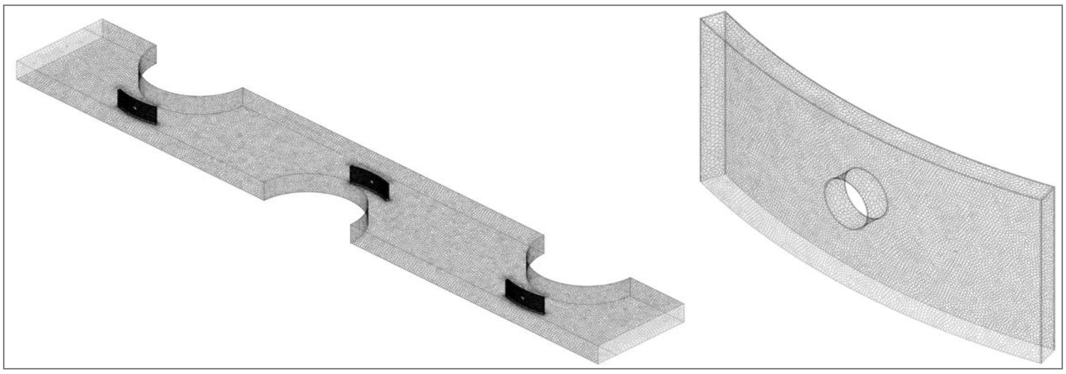

Figure 3. Computational grid test

2.6. Numerical Solution Methodology

Numerical simulations were performed under steady-state conditions using the finite volume method to solve the 3D governing equations of mass, momentum and energy. Airflow was assumed to be incompressible, Newtonian and turbulent, with constant thermophysical properties.

Turbulence effects were modelled using the shear stress transport (SST) k–ωmodel, which combines the robustness of the k–ωformulation near the wall with the freestream independence of the k–εmodel in the outer region. This model is particularly suitable for predicting adverse pressure gradients and flow separation occurring in fin–tube heat exchangers equipped with CRW-VGs.

The governing equations were discretised using a second-order upwind scheme for the convective terms of momentum and energy equations to enhance numerical accuracy. Pressure–velocity coupling was achieved using the SIMPLE algorithm. Spatial discretisation was applied consistently across the computational domain to ensure numerical stability.

A non-uniform computational grid was employed, with mesh refinement and inflation layers applied near the tube and VG surfaces to accurately capture velocity and thermal boundary layers. A grid independence study was conducted using four mesh resolutions, as detailed in **Table 1**. The variation in Nu_avg and f between the two finest meshes was less than 0.1%, indicating meshindependent results. Consequently, the mesh with 822,157 cells was selected for all simulations as an optimal compromise between accuracy and computational cost.

2.7. Validation

The convergence of the numerical solution was ensured by monitoring the normalised residuals of the governing equations. The convergence criteria were set to $10^{-5}$for continuity and momentum equations and 10^{-6} for the energy equation. In addition to residual reduction, global quantities, such as Nu_avg and pressure drop, were monitored to confirm the physical convergence of the solution.

The simulation model adopted in this study was based on a previously validated configuration [30], which serves as a reference case for assessing the reliability of the numerical method. Turbulent flow was modelled using the k–ω SST model in conjunction with the governing Eq. (1) to Eq. (3). This model is well known for accurately predicting adverse pressure gradients and flow separation, making it suitable for complex flow simulations in fin–tube heat exchangers equipped with curved VGs.

The numerical results were validated against published experimental data [30], as illustrated in **Figure 4**. The comparison showed good agreement, with deviations of 2%–6% for Nu and 4%–8% for f, and an overall error below 9%. These results confirm the reliability of the present numerical methodology for predicting heat exchanger performance.

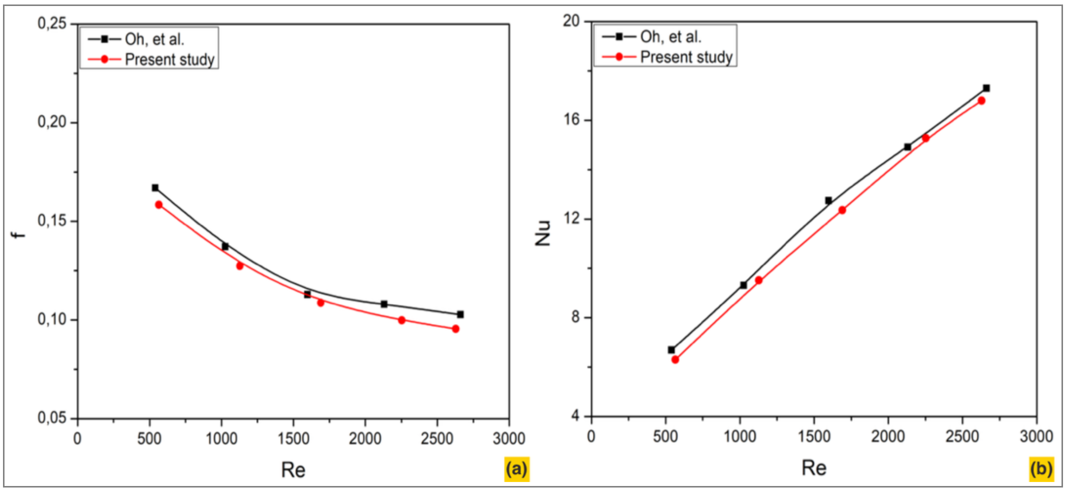

Figure 4. Numerical validation results: (a) *f*; (b) *Nu*

3. Results

3.1. Influence of Geometry and Radial Distance on the $\mathrm{Nu}/\mathrm{Nu_o}$ and $\mathrm{f}/\mathrm{f_o}$ Values

The assessment of heat transfer performance can be observed from the resulting Nu/Nu_o value. The comparison between Nu and Nu_o (Nusselt number under reference conditions) provides insight into heat transfer efficiency. Deviations in Nu/Nu_o signify alterations in the thermal performance of the observed system, as shown in **Figure 5** (i.e. (a) is 0.25 *H* and (b) is 0.5 *H*). **Figure 5** and **Figure 6** demonstrate the coupled relationship between heat transfer enhancement and flow resistance as a function of the attack angle, hole width and radial position of the CRW-VGs. As shown in **Figure 5**, the variation in Nu/Nu_o strongly depends on vortex stability and secondary flow development. At lower angles (30°–60°), moderate longitudinal vortices are generated, resulting in limited boundary layer disruption and moderate heat transfer enhancement. However, as indicated in **Figure 6**, this regime is accompanied by only a slight increase in f, reflecting a moderate disturbance level within the flow field.

When the angle approaches 75°–90°, both Nu/Nu_o (**Figure 5**) and f/f_o (**Figure 6**) reach relatively low values. This behaviour indicates a weakened and less coherent vortex structure, in which reduced mixing leads to minimal heat transfer enhancement and lowered flow resistance. The reduction in heat transfer in this region is mainly attributed to the reduced effective contact area for heat transfer, intensified rotational motion and the formation of lateral vortices on the surface of the perforated VGs [34], which dissipate energy without significantly enhancing boundary layer thinning.

A significant change occurs at 120°: a maximum Nu/Nu_0 (**Figure 5**) and a pronounced increase in f/f_0 (**Figure 6**). This correspondence confirms that strong and stable longitudinal vortices are formed at this angle, intensifying cross-stream mixing and effectively thinning the thermal boundary layer. However, enhanced vortex strength also increases shear stress and energy dissipation, leading to higher pressure penalties. This regime represents a high-disturbance, high-enhancement condition in which heat transfer improvement is achieved at the expense of increased friction losses.

At larger angles (135°–150°), both Nu/Nu_0 and f/f_0 decrease, suggesting vortex breakdown and excessive flow separation. Although flow disturbance remains present, the loss of vortex coherence reduces effective mixing and pressure buildup.

The influence of hole width and radial distance further clarifies the thermo-hydraulic interaction. The smaller hole width (0.25 *H*) produces more concentrated vortices and sharper enhancement peaks in **Figure 5** and relatively controlled friction increases in **Figure 6**. By contrast, the larger hole width (0.5 *H*) allows partial flow penetration through the perforation, promoting distributed secondary flows that increase energy dissipation and friction levels while slightly moderating heat transfer gains. Similarly, increasing the radial distance to r/R = 1.5 strengthens the vortex–wake interaction, enhancing Nu/Nu_0 but also elevating f/f_0 because of the intensified momentum exchange.

Overall, the combined analysis of **Figure 5** and **Figure 6** confirms that the thermo-hydraulic performance is governed by the balance between vortex intensity, boundary layer disruption and flow resistance. The angle of 120° emerges as the most effective configuration in terms of heat transfer enhancement, although its practical suitability must be evaluated through an integrated metric, such as the TEF, to ensure that the gain in heat transfer justifies the associated pressure penalty.

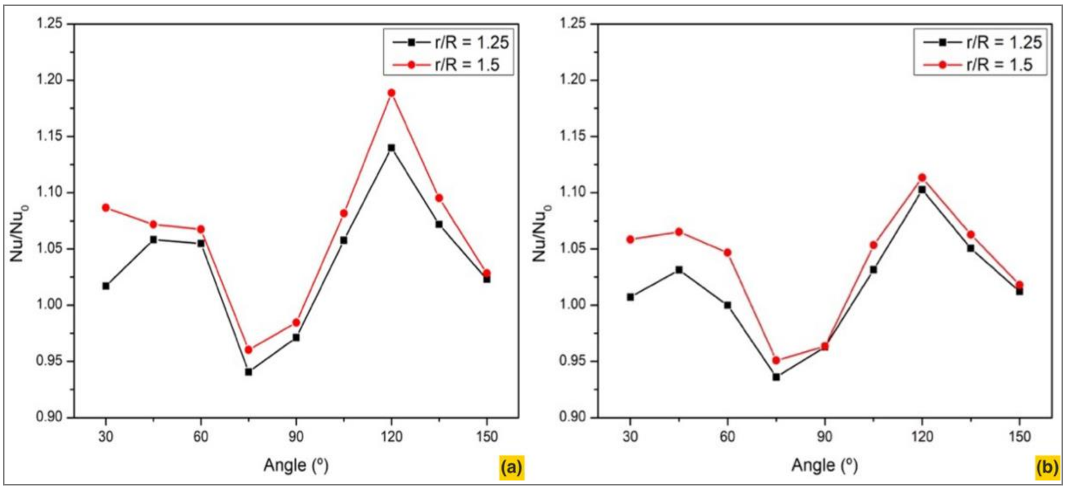

Figure 5. The effect Nu/Nu_o: (a) Hole width CRW-VGs 0.25*H*; (b) Hole width CRW-VGs 0.5*H*

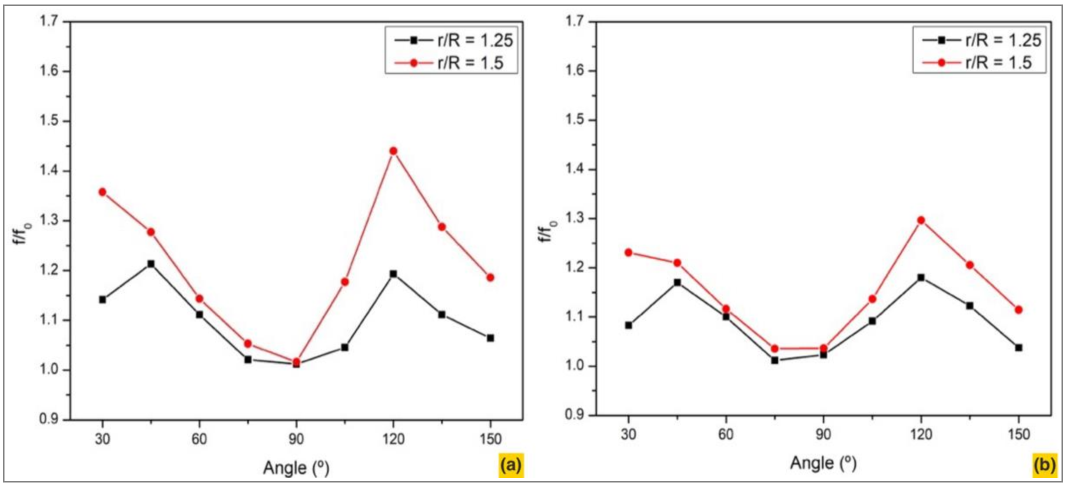

Figure 6. The effect of position angle on the friction factor: (a) Hole width CRW-VGs 0.25*H*; (b) Hole width CRW-VGs 0.5*H*

3.2. Flow Field and Thermal Field Interpretation

Reducing *f* with an increase in *Nu* using holes can reduce the pressure drop. As *Nu* and *f* are parameters of the TEF, the heat transfer performance can be determined, as discussed above, by looking at the contour changes in speed, temperature and pressure in **Figure 7** to **Figure 12**. **Figure 7** to **Figure 12** reveal that the thermo-hydraulic performance of the CRW-VGs is governed not merely by geometric variation but primarily by the stability regime of the generated longitudinal vortices. Three distinct flow regimes can be identified as the attack angle (α) increases: (i) weak vortex regime (30°–60°), (ii) coherent vortex amplification regime (75°–120°) and (iii) vortex breakdown regime (135°–150°).

In the weak vortex regime, velocity contours (**Figure 7** and **Figure 8**) indicate limited secondary flow development and only a partial disruption of the boundary layer. The generated vortices are insufficient to induce the deep penetration of core flow towards the heated surface.

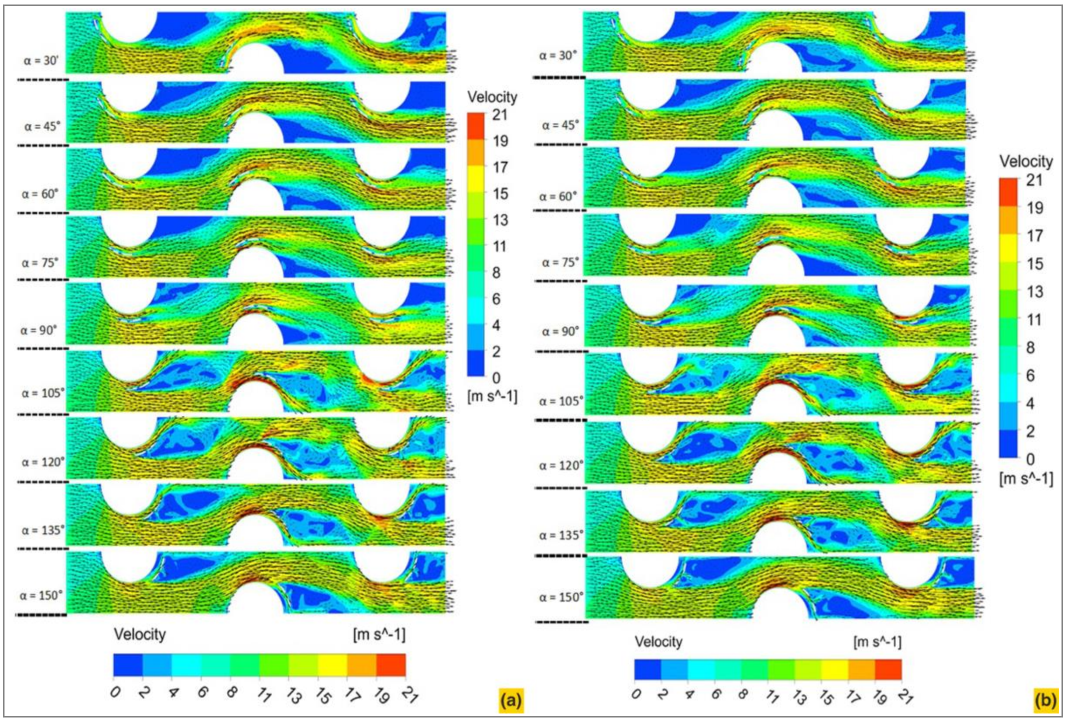

Figure 7. Velocity contour *r/R* 1.25: (a) Hole width 0.25*H*; (b) Hole width 0.5*H*

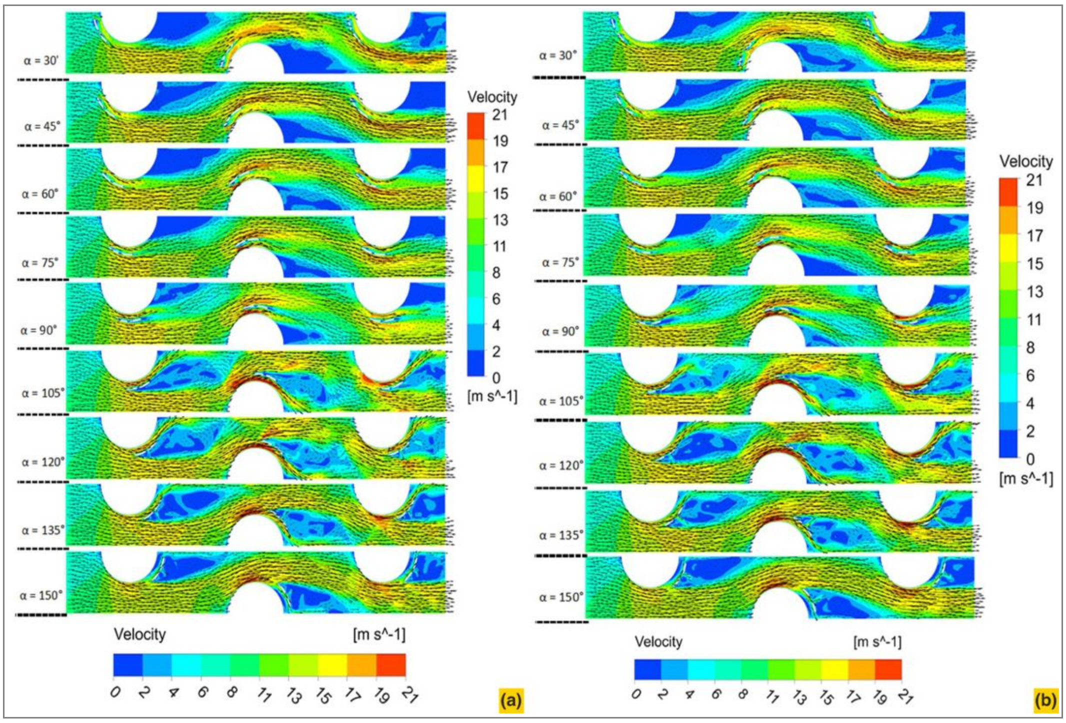

Figure 8. Velocity contour *r/R* 1.5: (a) Hole width 0.25*H*; (b) Hole width 0.5*H*

Consequently, the temperature contours (**Figure 11** and **Figure 12**) show a relatively thick thermal boundary layer and non-uniform temperature stratification. The pressure contours (**Figure 9** and **Figure 10**) display moderate upstream–downstream gradients, indicating limited energy dissipation and relatively small pressure penalties. However, as fluids move swiftly, they have fewer opportunities for prolonged interaction, resulting in smaller pressure drops [35]. This explains why lower attack angles, despite smoother flow behaviour, do not generate substantial convective enhancement.

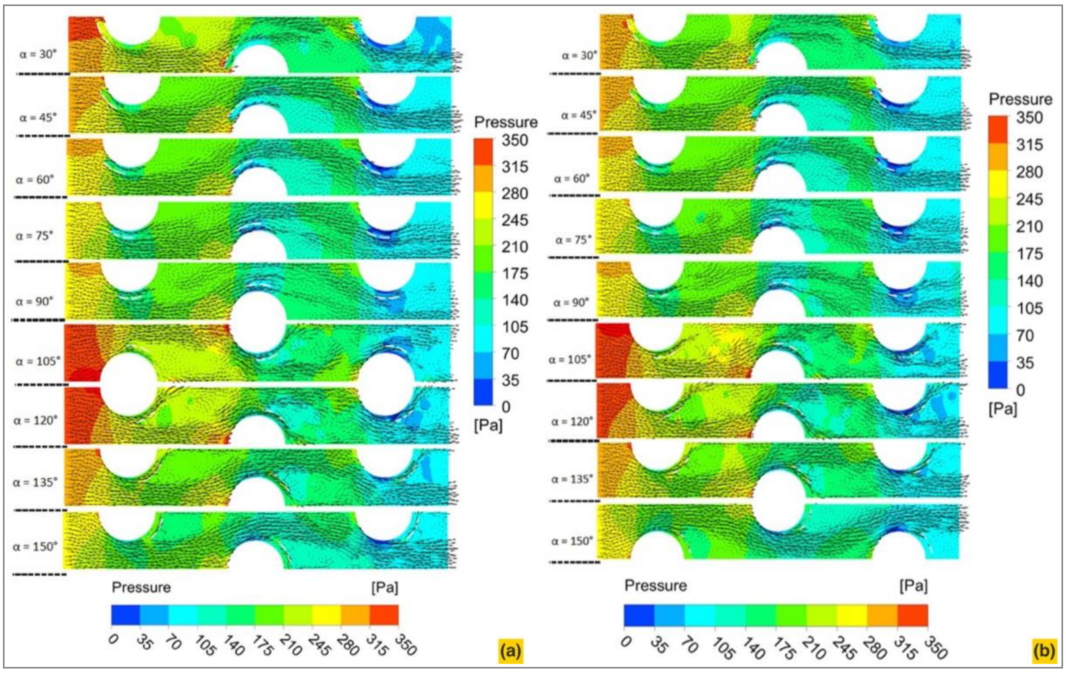

Figure 9.
Pressure drop contour *r/R* 1.25:
(a) Hole width 0.25*H*;
(b) Hole width 0.5*H*

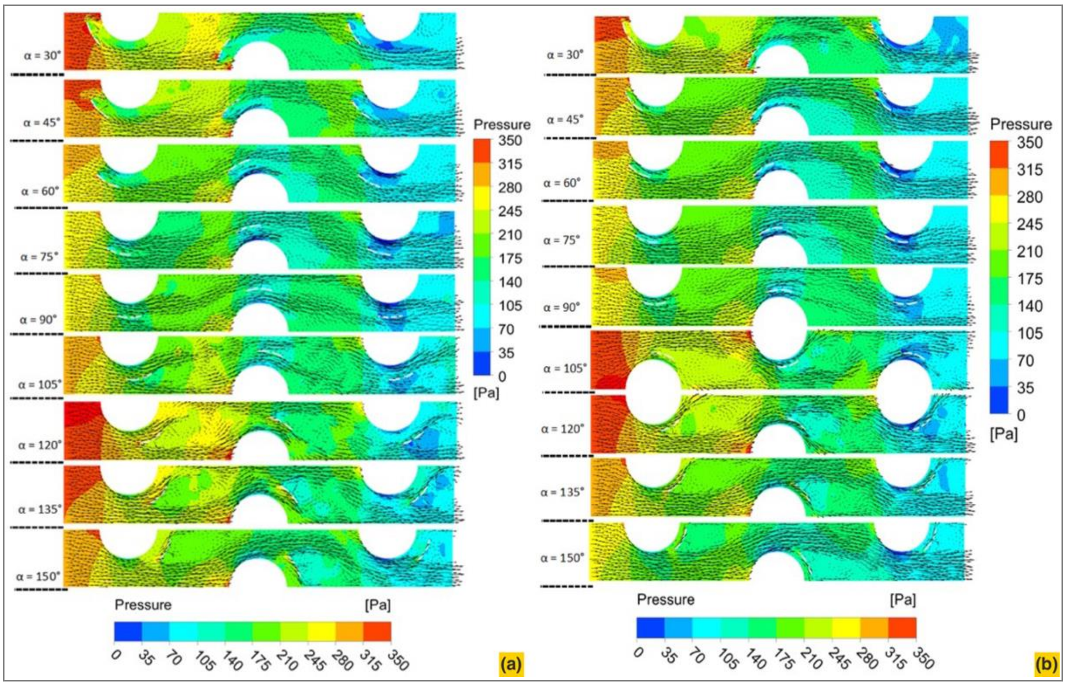

Figure 10.
Pressure drop contour *r/R* 1.5:
(a) Hole width 0.25*H*;
(b) Hole width 0.5*H*

A fundamentally different behaviour emerges in the coherent vortex amplification regime (α ≈ 105°–120°). In this range, the velocity field exhibits highly organised longitudinal vortices with an intensified cross-stream momentum exchange. The vortices transport high-momentum core fluid towards the heated wall while ejecting low-momentum near-wall fluid outward, significantly thinning the thermal boundary layer. The temperature distribution becomes more uniform, thus confirming enhanced convective transport. Simultaneously, the pressure field exhibits the most pronounced gradients, reflecting maximal shear production and vortex strength.

Nevertheless, the perforated configuration introduces an additional mechanism. As depicted in **Figure 9** and **Figure 10**, the jet stream emanating from the orifice of the CRW-VGs has the potential to alleviate stagnation flow, consequently reducing the pressure drop [36], [37], [38]. This jet-induced acceleration redistributes local pressure peaks and mitigates excessive recirculation behind the VG, thereby partially compensating for the pressure penalty associated with strong vortex generation. Therefore, this regime represents a critical transition state in which vortex strength and structural coherence are maximised, while perforation-induced jet flow moderates stagnation-related losses.

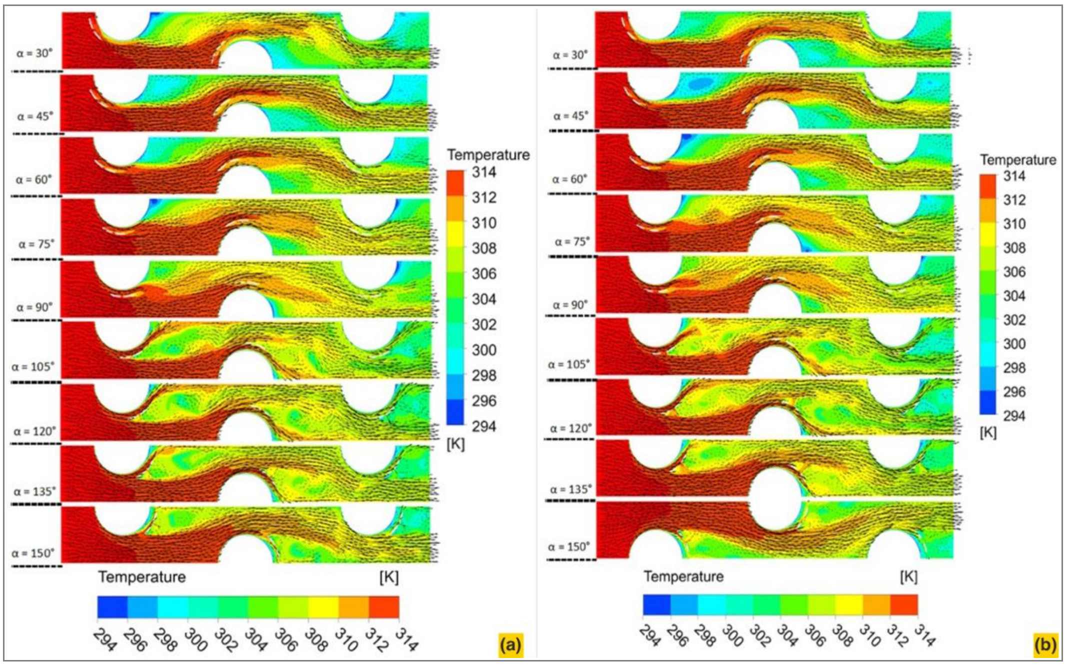

Figure 11. Temperature contour r/R 1.25: (a) Hole width 0.25H; (b) Hole width 0.5H

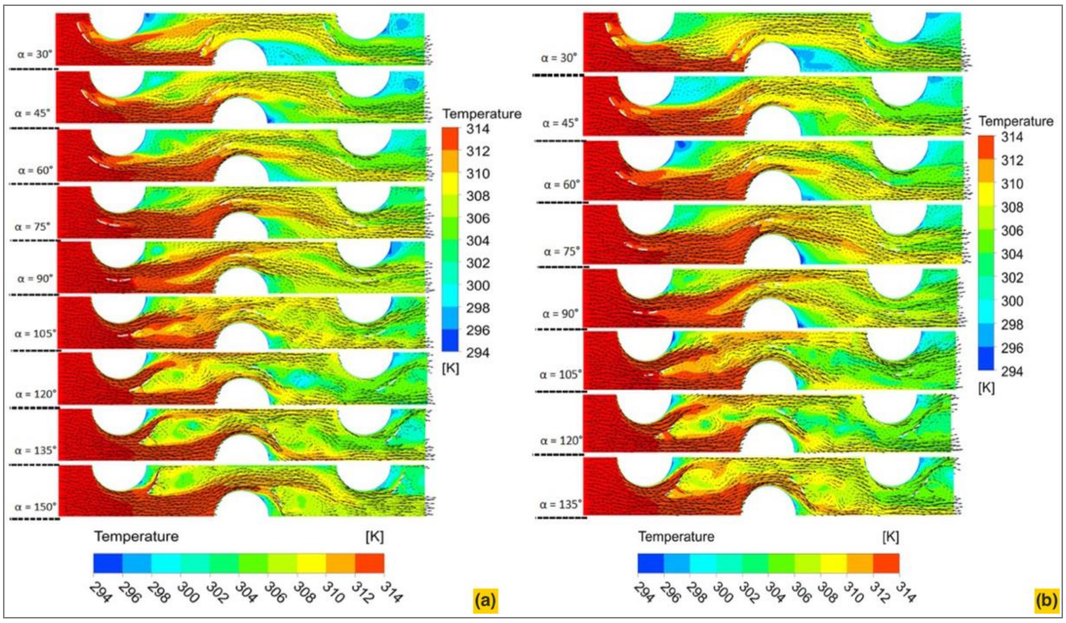

Figure 12. Temperature contour r/R 1.5: (a) Hole width 0.25H; (b) Hole width 0.5H

When α ≥ 135°, the system enters a vortex breakdown regime. Although apparent disturbance increases, velocity contours reveal fragmented and unstable vortical structures. The pressure distribution becomes spatially irregular, indicating that kinetic energy is increasingly dissipated through chaotic separation rather than organised secondary motion. As a result, temperature contours show reduced effectiveness in boundary layer thinning, despite intensified disturbance. This demonstrates that excessive geometric forcing shifts the system from a structured convective enhancement to instability-driven dissipation.

The geometric parameters further modulate these mechanisms. An increasing radial position to r/R = 1.5 enhances the wake–vortex interaction and prolongs vortex persistence, intensifying the heat transfer but also elevating the pressure penalties. Similarly, a smaller hole width (0.25 *H*) generates concentrated vortices and sharper shear layers, thereby promoting a stronger boundary layer disruption. By contrast, a larger hole width (0.5 *H*) allows for greater flow penetration through the perforation, redistributing vortex energy and stabilising the pressure field, thereby offering a more balanced thermo-hydraulic response.

Overall, the results demonstrate that thermo-hydraulic optimization is governed by vortex coherence rather than vortex magnitude alone. The optimal configuration (α ≈ 105°–120°) corresponds to the condition where organized secondary flow production is maximized, stagnation effects are partially mitigated by jet-induced flow through perforations, and instability-driven energy dissipation has not yet dominated the system. This mechanistic interpretation advances the understanding of perforated vortex generators by identifying vortex stability and jet–wake interaction as the primary control parameters governing performance. As illustrated in **Figure 13**, the streamline and velocity contours reveal a coherent high-velocity core developing along the inner wall of the curved channel, accompanied by jet-induced momentum injection from the perforations into the wake region. This mechanism promotes thermal boundary layer thinning through enhanced near-wall acceleration while simultaneously suppressing large-scale recirculation that would otherwise increase frictional losses. The interaction between curvature-driven Dean vortices and the longitudinal vortices generated by the VG further intensifies transverse momentum exchange, improving convective transport uniformity along the heated surface. Consequently, the heat transfer augmentation achieved within the optimal angular range is not merely a function of vortex strength, but rather of sustained vortex organization and controlled jet–wake stabilization, which collectively ensure enhanced Nusselt number performance with moderated pressure penalties.

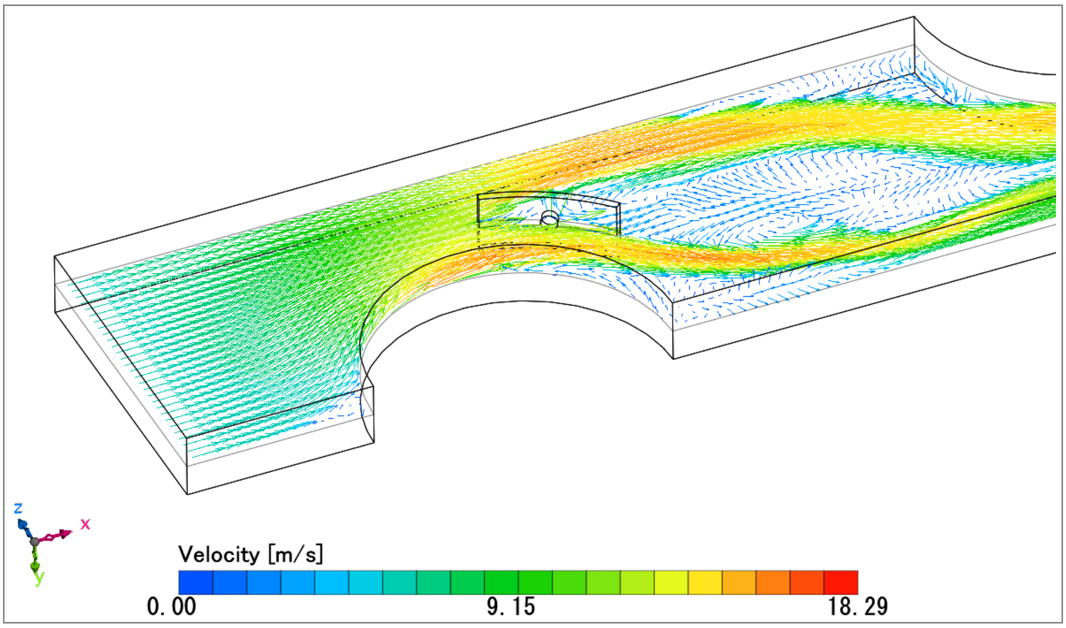

Figure 13. Streamline velocity α = 120°, *r/R* = 1.25, hole width = 0.5*H*

3.3. Influence of Geometry and Radial Distance on Thermal Enhancement Factor

The variation in the TEF with the r/R ratio at different angular positions is presented in **Figure 14a** and **Figure 14b** for hole widths of 0.25 *H* and 0.5 *H*, respectively. For both configurations, r/R = 1.25 consistently produces higher TEF values than r/R = 1.5, with the most pronounced improvement occurring at α = 120°. The maximum TEF reaches 1.075 for 0.25 *H* and 1.064 for 0.5 *H*. This trend indicates that a shorter radial distance provides a more favourable balance between heat transfer augmentation and friction penalty.

The superior performance at r/R = 1.25 is associated with a more effective vortex–jet interaction and controlled suppression of mixed-vortex interference. At α ≈ 120°, the wake region behind the tube is significantly weakened, promoting enhanced near-wall momentum exchange and boundary-layer disruption. Such overlapping vortex configurations signal a shift towards a more intensified turbulent regime [39], which is known to strengthen convective heat transfer mechanisms [40].

Although larger radial spacing intensifies vortex structures, it also increases flow resistance, thereby reducing the overall TEF, despite higher local heat transfer rates. The combined trends of Nu/Nu_0 and f/f_0 confirm that optimal thermo-hydraulic performance is governed by the synergy between vortex positioning, jet reinforcement and wake suppression rather than vortex strength alone.

The combined analysis of Nu/Nu_0 and f/f_0 (**Figure 5** and **Figure 12**) supports this behaviour. Increasing hole width reduces f, thereby mitigating the pressure drop, consistent with previous findings [41]. The jet streams generated by the CRW-VGs alleviate stagnant flow regions, particularly between 30° and 90°, while beyond 105°, the interaction between intensified vortices and wake dynamics temporarily elevates the pressure drop before stabilising near 120°. The temperature contours further confirm that higher angular positions weaken the recirculation zone and enhance thermal mixing.

Overall, the TEF distribution in **Figure 14** demonstrates that thermo-hydraulic optimisation is governed not only by vortex strength but also by the synergy between vortex positioning, jet reinforcement and wake suppression. The peak performance at r/R = 1.25 and α = 120° highlights the importance of geometric tuning to achieve maximum heat transfer enhancement with controlled hydraulic losses. These findings provide deeper physical insight into jet-assisted vortex dynamics and offer practical guidance for optimising VG placement in compact heat exchanger applications.

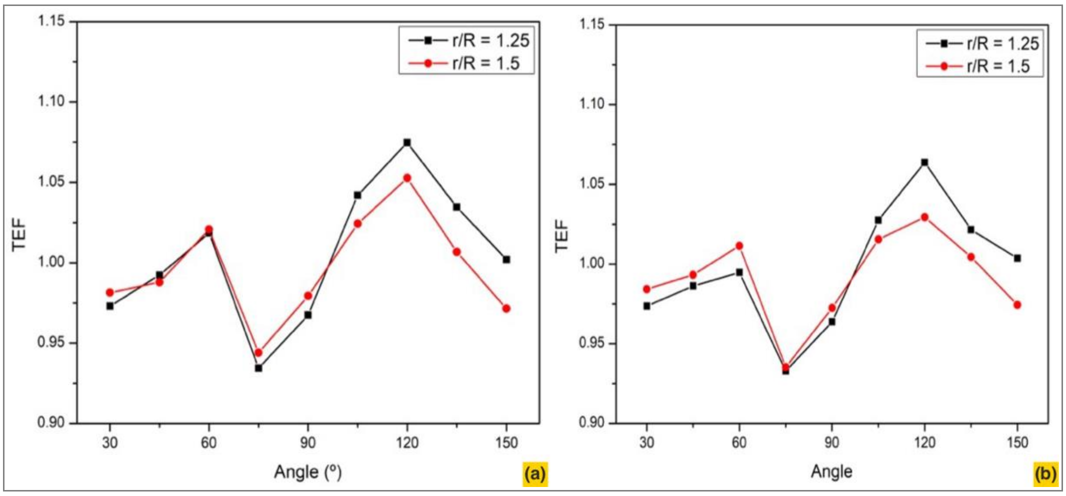

Figure 14. Thermal enhancement factor graph: (a) RWVGs hole width 0.25*H*; (b) RWVGs hole width 0.5*H*

3.4. Economic and Practical Implications of Thermal Enhancement Factor

The maximum TEF obtained in the present study is approximately 1.075, corresponding to a net thermo-hydraulic improvement of about 7%–8% under constant fan power conditions. Although this enhancement may appear moderate compared with some studies reporting TEF values in the range of 1.2–1.5 [42], [43], [44], it is important to recognise that such higher values are often associated with substantial pressure penalties or aggressive vortex geometries that may not be suitable for practical air-side applications. In fin–tube heat exchangers operating with low-density air, even a 5%–10% improvement in overall performance is practically meaningful, as it can reduce the required heat transfer surface area for a given thermal duty, improve compactness or lower long-term fan energy consumption [45], [46], [47].

From a manufacturing standpoint, the proposed perforated CRW-VGs are passive devices integrated directly with the fin structure and fabricated from thin sheet material. The addition of perforations does not introduce significant production complexity and can be implemented using conventional stamping or punching techniques commonly employed in fin manufacturing. Consequently, the incremental fabrication cost is expected to be minimal, particularly in large-scale production.

Moreover, the perforated configuration helps mitigate an excessive increase in pressure compared with solid VGs, thereby reducing aerodynamic loading on the fan system. The resulting balance between heat transfer enhancement and controlled friction penalty demonstrates that the proposed design achieves realistic thermo-hydraulic optimisation rather than maximum vortex intensity alone. Although a comprehensive life-cycle cost analysis is beyond the scope of this numerical study, the combination of TEF greater than unity, moderate pressure penalties and low manufacturing complexity supports the technical relevance and economic feasibility of the proposed configuration for practical Heating, Ventilation, and Air Conditioning and compact thermal management applications.

4. Conclusions

This study reveals that the thermo-hydraulic performance of CRW-VGs is governed by the interaction between vortex positioning, jet momentum and wake suppression rather than vortex strength alone. The results explicitly show that a shorter radial distance (r/R = 1.25) provides a more favourable balance between heat transfer enhancement and pressure penalty than r/R = 1.5. Although larger radial spacing intensifies vortex structures and increases Nu/Nu_0, the accompanying increase in f reduces the overall TEF.

The optimal angular position is identified at α = 120°, at which the wake region behind the tube is significantly weakened. This configuration promotes a stronger near-wall momentum exchange, a more uniform boundary-layer disruption and improved thermal mixing. The TEF reaches its maximum values of 1.075 (0.25 *H*) and 1.064 (0.5 *H*) under this condition, confirming that wake restructuring plays a decisive role in thermo-hydraulic optimisation.

Furthermore, increasing the feeding hole width enhances jet strength, which intensifies turbulence and redistributes momentum more effectively. More importantly, this jet-assisted mechanism contributes not only to heat transfer augmentation but also to moderating pressure losses, demonstrating that momentum redistribution is more critical than simply increasing vortex intensity.

Overall, the findings establish that the optimal CRW-VG design requires controlled vortex suppression, strategic angular positioning and jet reinforcement to achieve maximum TEF. These results provide mechanistic insight into jet–vortex synergy and offer practical guidance for high-efficiency compact heat exchanger design.

Acknowledgements

The author extends gratitude to Office of Research UHAMKA for support for this research and to the Office of Publication of UHAMKA for their assistance in providing technical guidance. This research was not funded by any grant.

Authors' Declaration

Authors' contributions and responsibilities – The authors made substantial contributions to the conception and design of the study. The authors took responsibility for data analysis, interpretation and discussion of results. The authors read and approved the final manuscript.

Funding – This research was not funded by any grant.

Availability of data and materials – All data is available from the authors.

Competing interests – The authors declare no competing interests.

Additional information – No additional information from the authors.

Nomenclature

D	: Tube diameter (m)	r	: Radial distance of VG from tube center (m)
f	: Darcy friction factor (–)	R	: Tube radius (m)
f_0	: Friction factor without vortex generator (–)	T	: Static temperature (K)
H	: Channel height (m)	T_{in}	: Inlet air temperature (K)
k	: Thermal conductivity of air (W m^{-1} K^{-1})	T_w	: Tube wall temperature (K)
L	: Tube length (m)	α	: Angular position of vortex generator (degree)
N_u	: Nusselt number (–)	μ	: Dynamic viscosity (Pa s)
Nu_{avg}	: Average Nusselt number (–)	ρ	: Air density (kg m^{-3})
Nu_0	: Nusselt number without vortex generator (–)	r/R	: Radial distance ratio (–)
P	: Static pressure (Pa)	Nu/Nu_0	: Nusselt number ratio (–)
P_L	: Longitudinal pitch (m)	f/f_0	: Friction factor ratio (–)
P_T	: Transverse pitch (m)	TEF	: Thermal enhancement factor (–)

References

[1] K. Torii, K. M. Kwak, and K. Nishino, “Heat transfer enhancement accompanying pressure-loss reduction with winglet-type vortex generators for fin-tube heat exchangers,” *International Journal of Heat and Mass Transfer*, vol. 45, no. 18, pp. 3795–3801, Aug. 2002, doi: 10.1016/S0017-9310(02)00080-7.

[2] P. T. Tsilingiris, “Review and critical comparative evaluation of moist air thermophysical properties at the temperature range between 0 and 100 °C for Engineering Calculations,” *Renewable and Sustainable Energy Reviews*, vol. 83, pp. 50–63, Mar. 2018, doi: 10.1016/j.rser.2017.10.072.

[3] Dan Mugisidi, Oktarina Heriyani, Pancatatva Hesti Gunawan, and Dwi Apriani, “Performance Improvement of a Forced Draught Cooling Tower Using a Vortex Generator,” *CFD Letters*, vol. 13, no. 1, pp. 45–57, Jan. 2021, doi: 10.37934/cfdl.13.1.4557.

[4] Syaiful, H. Nabilah, M. S. K. T. Suryo Utomo, A. Suprihanto, and M. F. Soetanto, “Numerical simulation of heat transfer enhancement from tubes surface to airflow using concave delta winglet vortex generators,” *Results in Engineering*, vol. 16, p. 100710, Dec. 2022, doi: 10.1016/j.rineng.2022.100710.

[5] M. Awais and A. A. Bhuiyan, “Heat transfer enhancement using different types of vortex generators (VGs): A review on experimental and numerical activities,” *Thermal Science and Engineering Progress*, vol. 5, pp. 524–545, Mar. 2018, doi: 10.1016/j.tsep.2018.02.007.

[6] S. K. Sarangi and D. P. Mishra, “Effect of winglet location on heat transfer of a fin-and-tube heat exchanger,” *Applied Thermal Engineering*, vol. 116, pp. 528–540, Apr. 2017, doi: 10.1016/j.applthermaleng.2017.01.106.

[7] K. Song, Z. Xi, M. Su, L. Wang, X. Wu, and L. Wang, “Effect of geometric size of curved delta winglet vortex generators and tube pitch on heat transfer characteristics of fin-tube heat exchanger,” *Experimental Thermal and Fluid Science*, vol. 82, pp. 8–18, Apr. 2017, doi: 10.1016/j.expthermflusci.2016.11.002.

[8] A. Boonloi and W. Jedsadaratanachai, “Air Flow, Thermal Profile, and Thermohydraulic Performance Assessment in a Square Duct Heat Exchanger With Combined Vortex Generators: CFD Analysis,” *Journal of Engineering*, vol. 2025, no. 1, Jan. 2025, doi: 10.1155/je/4197880.

[9] H. Karkaba, T. Dbouk, C. Habchi, S. Russeil, T. Lemenand, and D. Bougeard, “Multiobjective optimization of Vortex Generators for heat transfer enhancement in turbulent flows,” *International Journal of Thermofluids*, vol. 22, p. 100633, May 2024, doi: 10.1016/j.ijft.2024.100633.

[10] H. Arjmandi, R. Amini, A. Ghaffari, H. Rahmani, and A. Chamkha, “Effects of baffles and vortex generators on cooling performance of a gas turbine combustion chamber: Numerical assessment,” *Alexandria Engineering Journal*, vol. 61, no. 6, pp. 4467–4478, Jun. 2022, doi: 10.1016/j.aej.2021.10.005.

[11] U. Kashyap, K. Das, and B. K. Debnath, “Effect of surface modification of a rectangular vortex generator on heat transfer rate from a surface to fluid: An extended study,” *International Journal of Thermal Sciences*, vol. 134, pp. 269–281, Dec. 2018, doi: 10.1016/j.ijthermalsci.2018.08.020.

[12] H. Naik and S. Tiwari, “Effect of winglet location on performance of fin-tube heat exchangers with inline tube arrangement,” *International Journal of Heat and Mass Transfer*, vol. 125, pp. 248–261, Oct. 2018, doi: 10.1016/j.ijheatmasstransfer.2018.04.071.

[13] Z. Qian, Q. Wang, and J. Cheng, “Analysis of heat and resistance performance of plate fin-and-tube heat exchanger with rectangle-winglet vortex generator,” *International Journal of Heat and Mass Transfer*, vol. 124, pp. 1198–1211, Sep. 2018, doi: 10.1016/j.ijheatmasstransfer.2018.04.037.

[14] K. Srivastava and R. R. Sahoo, “Effect of pitch and angle of attack on thermal performance of new envelope and delta vortex generators for TEG: An experimental and numerical approach,” *International Journal of Thermal Sciences*, vol. 195, p. 108671, Jan. 2024, doi: 10.1016/j.ijthermalsci.2023.108671.

[15] C. Luo, S. Wu, K. Song, L. Hua, and L. Wang, “Thermo-hydraulic performance optimization of wavy fin heat exchanger by combining delta winglet vortex generators,” *Applied Thermal

Engineering, vol. 163, p. 114343, Dec. 2019, doi: 10.1016/j.applthermaleng.2019.114343.

[16] O. Heriyani, M. Djaeni, Syaiful, and A. K. Putri, "Perforated concave rectangular winglet pair vortex generators enhance the heat transfer of air flowing through heated tubes inside a channel," *Results in Engineering*, vol. 16, p. 100705, Dec. 2022, doi: 10.1016/j.rineng.2022.100705.

[17] M. Dogan and S. Erzincan, "Experimental investigation of thermal performance of novel type vortex generator in rectangular channel," *International Communications in Heat and Mass Transfer*, vol. 144, p. 106785, May 2023, doi: 10.1016/j.icheatmasstransfer.2023.106785.

[18] Z. Ke, C.-L. Chen, K. Li, S. Wang, and C.-H. Chen, "Vortex dynamics and heat transfer of longitudinal vortex generators in a rectangular channel," *International Journal of Heat and Mass Transfer*, vol. 132, pp. 871–885, Apr. 2019, doi: 10.1016/j.ijheatmasstransfer.2018.12.064.

[19] H. Fu, H. Sun, L. Yang, L. Yan, Y. Luan, and F. Magagnato, "Effects of the configuration of the delta winglet longitudinal vortex generators and channel height on flow and heat transfer in minichannels," *Applied Thermal Engineering*, vol. 227, p. 120401, Jun. 2023, doi: 10.1016/j.applthermaleng.2023.120401.

[20] J. Batista, A. Trp, K. Lenic, and M. Kirincic, "The influence of geometry parameters of rectangular vortex generators on the air-to-water fin-and-tube heat exchanger efficiency enhancement," *International Communications in Heat and Mass Transfer*, vol. 162, p. 108647, Mar. 2025, doi: 10.1016/j.icheatmasstransfer.2025.108647.

[21] D. Jin, S. Quan, J. Zuo, and S. Xu, "Numerical investigation of heat transfer enhancement in a solar air heater roughened by multiple V-shaped ribs," *Renewable Energy*, vol. 134, pp. 78–88, Apr. 2019, doi: 10.1016/j.renene.2018.11.016.

[22] S. Pourhedayat, S. M. Pesteei, H. E. Ghalinghie, M. Hashemian, and M. A. Ashraf, "Thermal-exergetic behavior of triangular vortex generators through the cylindrical tubes," *International Journal of Heat and Mass Transfer*, vol. 151, p. 119406, Apr. 2020, doi: 10.1016/j.ijheatmasstransfer.2020.119406.

[23] J. Wang, L. Zeng, T. Fu, S. Yu, and Y. He, "Effects of the position and perforation parameters of the delta winglet vortex generators on flow and heat transfer in minichannels," *International Journal of Thermal Sciences*, vol. 198, p. 108878, Apr. 2024, doi: 10.1016/j.ijthermalsci.2023.108878.

[24] P. Promvonge and S. Skullong, "Heat transfer augmentation in solar receiver heat exchanger with hole-punched wings," *Applied Thermal Engineering*, vol. 155, pp. 59–69, Jun. 2019, doi: 10.1016/j.applthermaleng.2019.03.132.

[25] M. E. Nakhchi, M. Hatami, and M. Rahmati, "Experimental investigation of performance improvement of double-pipe heat exchangers with novel perforated elliptic turbulators," *International Journal of Thermal Sciences*, vol. 168, p. 107057, Oct. 2021, doi: 10.1016/j.ijthermalsci.2021.107057.

[26] A. J. Modi, N. A. Kalel, and M. K. Rathod, "Thermal performance augmentation of fin-and-tube heat exchanger using rectangular winglet vortex generators having circular punched holes," *International Journal of Heat and Mass Transfer*, vol. 158, p. 119724, Sep. 2020, doi: 10.1016/j.ijheatmasstransfer.2020.119724.

[27] Z. Han, Z. Xu, and J. Wang, "Numerical simulation on heat transfer characteristics of rectangular vortex generators with a hole," *International Journal of Heat and Mass Transfer*, vol. 126, pp. 993–1001, Nov. 2018, doi: 10.1016/j.ijheatmasstransfer.2018.06.081.

[28] J. Wang, T. Fu, L. Zeng, F. Lien, and G. Chen, "Thermal-hydraulic performance in a tube with punched delta winglets inserts in turbulent flow," *International Journal of Thermal Sciences*, vol. 172, p. 107326, Feb. 2022, doi: 10.1016/j.ijthermalsci.2021.107326.

[29] P. Saini and M. P. Shah, "Performance evaluation of finned tube heat exchanger using curved wavy delta winglet vortex generators with circular perforations," *International Communications in Heat and Mass Transfer*, vol. 159, p. 108184, Dec. 2024, doi: 10.1016/j.icheatmasstransfer.2024.108184.

[30] Y. Oh and K. Kim, "Effects of position and geometry of curved vortex generators on fin-tube heat-exchanger performance characteristics," *Applied Thermal Engineering*, vol. 189, p. 116736, May 2021, doi: 10.1016/j.applthermaleng.2021.116736.

[31] M.-W. Tian, S. Khorasani, H. Moria, S. Pourhedayat, and H. S. Dizaji, “Profit and efficiency boost of triangular vortex-generators by novel techniques,” *International Journal of Heat and Mass Transfer*, vol. 156, p. 119842, Aug. 2020, doi: 10.1016/j.ijheatmasstransfer.2020.119842.

[32] P. Knödler and V. Dreissigacker, “Fluid Dynamic Assessment and Development of Nusselt Correlations for Fischer Koch S Structures,” *Energies*, vol. 17, no. 3, p. 688, Jan. 2024, doi: 10.3390/en17030688.

[33] X. Zou, S. B. Lo, R. Sevilla, O. Hassan, and K. Morgan, “The generation of tetrahedral meshes for NURBS-enhanced FEM,” *Engineering with Computers*, vol. 40, no. 6, pp. 3949–3977, Dec. 2024, doi: 10.1007/s00366-024-02004-z.

[34] P. Saini, A. Dhar, and S. Powar, “Performance enhancement of fin and tube heat exchanger employing curved delta winglet vortex generator with circular punched holes,” *International Journal of Thermofluids*, vol. 20, p. 100452, Nov. 2023, doi: 10.1016/j.ijft.2023.100452.

[35] M. K. Fahad, N. F. Ifraj, S. H. Tahsin, and M. J. Hasan, “Numerical investigation of the hydrothermal performance of novel vortex generators in a rectangular channel by employing inclination and rotational angles,” *International Journal of Thermofluids*, vol. 20, p. 100500, Nov. 2023, doi: 10.1016/j.ijft.2023.100500.

[36] S. Gururatana and S. Skullong, “Heat transfer augmentation in a pipe with 3D printed wavy insert,” *Case Studies in Thermal Engineering*, vol. 21, p. 100698, Oct. 2020, doi: 10.1016/j.csite.2020.100698.

[37] A. Sinha, H. Chattopadhyay, A. K. Iyengar, and G. Biswas, “Enhancement of heat transfer in a fin-tube heat exchanger using rectangular winglet type vortex generators,” *International Journal of Heat and Mass Transfer*, vol. 101, pp. 667–681, Oct. 2016, doi: 10.1016/j.ijheatmasstransfer.2016.05.032.

[38] D. Hu *et al.*, “Performance optimization of a wavy finned-tube heat exchanger with staggered curved vortex generators,” *International Journal of Thermal Sciences*, vol. 183, p. 107830, Jan. 2023, doi: 10.1016/j.ijthermalsci.2022.107830.

[39] K. Srivastava and R. R. Sahoo, “Experimental and numerical study on thermal performance of new envelope and triangular vortex generators with different pitch and angle of attack,” *Thermal Science and Engineering Progress*, vol. 49, p. 102459, Mar. 2024, doi: 10.1016/j.tsep.2024.102459.

[40] A. J. Modi and M. K. Rathod, “Experimental investigation of heat transfer enhancement and pressure drop of fin-and-circular tube heat exchangers with modified rectangular winglet vortex generator,” *International Journal of Heat and Mass Transfer*, vol. 189, p. 122742, Jun. 2022, doi: 10.1016/j.ijheatmasstransfer.2022.122742.

[41] R. B. Pérez, A. M. Pérez, and D. S. Suárez, “Influence of the punched holes on thermohydraulic performance and flow pattern of rectangular channels with a pair of perforated vortex generators,” *International Journal of Heat and Mass Transfer*, vol. 184, p. 122291, Mar. 2022, doi: 10.1016/j.ijheatmasstransfer.2021.122291.

[42] J. Wang, L. Zeng, Y. He, B. Zhao, and P. Chu, “Effect of structure parameters on thermal performance of novel punched V-shape VGs for hear exchangers: An experimental approach,” *International Communications in Heat and Mass Transfer*, vol. 155, p. 107472, Jun. 2024, doi: 10.1016/j.icheatmasstransfer.2024.107472.

[43] J. Wang, C. Li, L. Zeng, T. Fu, and K. Liu, “Thermal performance analysis of a heat exchanger with a novel turbulator insert by using machine learning method,” *Case Studies in Thermal Engineering*, vol. 72, p. 106412, Aug. 2025, doi: 10.1016/j.csite.2025.106412.

[44] A. Boonloi and W. Jedsadaratanachai, “Turbulent forced convection in a square duct heat exchanger (SDHX) equipped with combined vortex turbulators (CVT): A numerical investigation,” *International Communications in Heat and Mass Transfer*, vol. 161, p. 108421, Feb. 2025, doi: 10.1016/j.icheatmasstransfer.2024.108421.

[45] W. Wei, G. Xu, Y. Wang, and E. Ding, “Study on air-side performance of air-cooled heat exchangers under large air velocity and wet conditions,” *Thermal Science and Engineering Progress*, vol. 48, p. 102389, Feb. 2024, doi: 10.1016/j.tsep.2024.102389.

[46] P. Yang, T. Qing, X. Lei, L. Wang, and Y. Liu, “Experimental study on thermal–hydraulic performance of moist air inside flat tube of two kinds of plate-fin heat exchangers,” *Applied Thermal Engineering*, vol. 239, p. 122121, Feb. 2024, doi:

10.1016/j.applthermaleng.2023.122121.

[47] M. H. Alshameri, A. A. Azizuddin, A. Arshad, H. G. Mohammed, and S. Sadeq, “Experimental Analysis of Thermal and Hydraulic Performance of Fiber-Reinforced Polymer Fins in Compact Heat Exchangers,” *International Journal of Automotive and Mechanical Engineering*, vol. 22, no. 2, pp. 12496–12510, Jun. 2025, doi: 10.15282/ijame.22.2.2025.18.0955.